Applied Energy xxx (2016) xxx–xxx

Contents lists available at ScienceDirect

Applied Energy

journal homepage: www.elsevier.com/locate/apenergy

A new maximum power point method based on a sliding mode approach for solar energy harvesting

Maissa Farhat [a,*], Oscar Barambones [b], Lassaad Sbita [a]

[a] Research Unit of Photovoltaic, Wind and Geothermal Systems, National Engineering School of Gabes, University of Gabes, Rue Omar Ibn-Elkhattab, Zrig, Gabès 6029, Tunisia
[b] Advanced Control Group, Universidad del País Vasco, EUI, Nieves Cano 12, 01006 Vitoria, Spain

HIGHLIGHTS

- Create a simple, easy of implement and accurate V_{MPP} estimator.
- Stability analysis of the proposed system based on the Lyapunov's theory.
- A comparative study versus P&O, highlight SMC good performances.
- Construct a new PS-SMC algorithm to include the partial shadow case.
- Experimental validation of the SMC MPP tracker.

ARTICLE INFO

Article history:
Received 14 August 2015
Received in revised form 5 March 2016
Accepted 16 March 2016
Available online xxxx

Keywords:
PV system
Practical implantation
Boost converter
MPPT
Sliding mode
Shadow

ABSTRACT

This paper presents a photovoltaic (PV) system with a maximum power point tracking (MPPT) facility. The goal of this work is to maximize power extraction from the photovoltaic generator (PVG). This goal is achieved using a sliding mode controller (SMC) that drives a boost converter connected between the PVG and the load. The system is modeled and tested under MATLAB/SIMULINK environment. In simulation, the sliding mode controller offers fast and accurate convergence to the maximum power operating point that outperforms the well-known perturbation and observation method (P&O). The sliding mode controller performance is evaluated during steady-state, against load varying and panel partial shadow (PS) disturbances. To confirm the above conclusion, a practical implementation of the maximum power point tracker based sliding mode controller on a hardware setup is performed on a dSPACE real time digital control platform. The data acquisition and the control system are conducted all around dSPACE 1104 controller board and its RTI environment. The experimental results demonstrate the validity of the proposed control scheme over a stand-alone real photovoltaic system.

1. Introduction

The fluctuations of rising oil prices and increasingly worrying degree of pollution contrasted with the new provisions of sustainable development make alternative and renewable energy sources more attractive. Economic incentives and huge advancement in electronic technology promote the use of photovoltaic systems. These systems present a simple and convenient solution from an economic point of view. The use of a converter on these photovoltaic systems is even more compelling as it increases their efficiency and reduces their costs.

This work analyses the control of a stand-alone PV system. The success of a PV application depends on weather conditions where the power electronic devices help to increase the efficiency of the PV generator (PVG). Extracting maximum power from the PVG is a challenge. Maximum power point tracking (MPPT) controller accuracy is a key control in the device operation for successful PV applications. In general, a PV system is typically built around the following main components as shown in Fig. 1:

(1) PVG that converts solar energy into electric energy.
(2) DC–DC converter that manipulates produced DC voltage by the PVG to feed a load voltage demand.
(3) Digital controller that drives the converter commutations accordingly to a MPPT capability.
(4) A load.

* Corresponding author.
E-mail addresses: maissa.farhat@gmail.com (M. Farhat), oscar.barambones@ehu.es (O. Barambones), lassaad.sbita@enig.rnu.tn (L. Sbita).

http://dx.doi.org/10.1016/j.apenergy.2016.03.055
0306-2619/

Nomenclature

G, G_{ref}	global, reference insulation (W/m^2)
I_p, V_p	cell output current and voltage
R_p, R_s	cell parallel and series resistance (Ω)
n, Eg	solar ideal factor and band gap energy (eV)
Irs	reverse diode saturation current (A)
K_{SCT}	short circuit current temperature (A/K)
T_c, T_{c_ref}	cell junction and Reference temperature (°C)
β, D	Boltzmann constant (1.38e−23) and duty cycle
Ns, Np	number of series and parallel modules
ns	number of series cells
k'	PS-SMC crisp value

In general, the MPPT control is challenging because the conditions that determine the amount of sun energy into the PVG may change at any time. As such, the PV system can be considered as non-linear complex.

Numerous MPPT methods have been developed and implemented in previous studies including [1], perturb and observe (P&O) [2], incremental conductance (Inc-Cond) [3], fractional open-circuit voltage and short circuit current [3], fuzzy logic controller (FLC) approaches [4], and Adaptive neuro fuzzy inference system, etc. [5]. These algorithms consist of introducing a crisp value, positive or negative (decrease or increase), all around the actual PVG operating point. From the previous power point position, the trajectory of the new command value helps the algorithm to decide on the command output value. These techniques have high tracking accuracy under stable conditions. It however still reveals some trade-offs between tracking speed and tracking reliability when load values or weather conditions rapidly change.

The sliding mode controller has recently attracted considerable attention from researchers due to several advantages [6,7], the main advantage of the SMC is its implementation simplicity, robustness, and great performance in different fields such as robotics [8] and motor control [9]. This work interest focused on the use of SMC in the photovoltaic fields by maximizing the power generated from the PV panels while maintaining the system stability.

This paper proposes a new design of stable SMC for PV system control. The proposed control methodology is built into two steps in order to control a PV system. The first step consists of an estimator synthesis of V_{ref}. This last corresponds to the (MPP) working voltage $V_{ref} = V_{MPP}$. The second is to perform the system tracking based on the developed SMC regulator for a boost converter and according to the estimated voltage value.

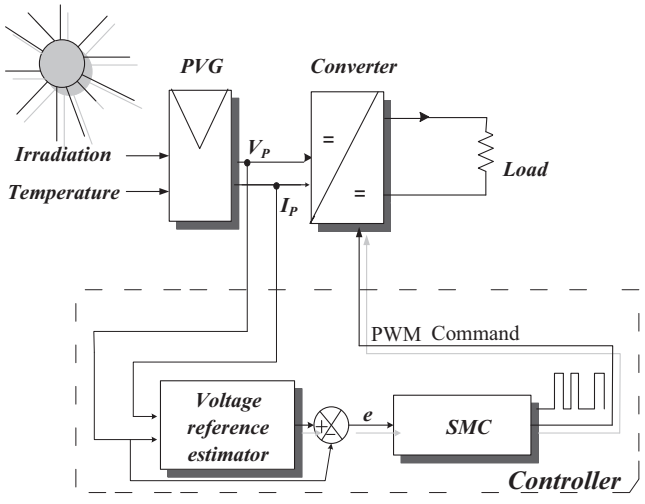

Fig. 1. Synoptic diagram of PVG system.

In previous work [5], the (V_{ref}) value can be provided only after the drawing of panel characteristics; however, this value will be valid only for a short period, so any change in weather will cause a change in its characteristics and as a result a change in the value of V_{MPP}. This method, as consequence, is valid only after determination of the right value of V_{MPP} [10,11]. The main objective in this work is to construct an MPP voltage-reference estimator that meets the MPP. The estimator is designed specifically in order to compute on-line the optimal voltage value V_{MPP}. In this paper, the proposed SMC uses the error between the measured voltage of the PV module and the voltage generated by the voltage reference estimator to adjust continuously the duty cycle (D) of the DC–DC Boost converter in order to eliminate this error. The reference voltage value is generated online with no need to know the actual irradiation. The PV system topology proposed is shown in Fig. 1. As shown in Fig. 1, the SMC algorithm directly generates the PWM signal. It has the benefit of avoid the use of the PWM commutation signal (Saw signal). It also permits the direct building of a PWM output signal toward the converter IGBT Gate. The SMC overcomes the limitations with other algorithms such as P&O [12] and Inc [13] which generates a duty cycle control value comparable to saw signal to uphold a PWM IGBT drive signal.

The performance of a photovoltaic module is highly affected by the partial shaded condition [14]. The PVG under partial shading makes maximum power point (MPP) tracking difficult; generally, there will exist multiple local MPPs, and their values will change as rapidly as the illumination [15]. Finding a solution to this problem ensures PVG power reliability and strengthens its economic rationale. Installers have an interest in resolving this issue. Many installers carefully design installations to avoid structural shading [16]. Installers could make a relatively effective strategy in order to avoid partial structural shading by carrying out a precise study of the proposed photovoltaic (PV) site of installation. The loss of energy caused by the PS is difficult to predict because it depends on several variables including internal module-interconnections [17].

Researchers and engineers developed an electronic solution to this problem by identifying and harvesting the maximum power of each panel individually using power optimizer technology [18], however, this method increases the cost of the installation. In addition, most MPPT are not able to get the maximum power point under these conditions.

Unconventional techniques have been recently widely used in literature for PS condition; authors in [19] use an MPPT managed by an adaptive neuro fuzzy inference system. Researcher in [20] uses ANN as an MPPT method for shading conditions. Although ANN and ANFIS have a good performance, they also present some drawbacks especially in rapid variation. Therefore, its robustness requires a huge database and consequently a long computing time and a large amount of memory. A speed/accuracy trade-off is therefore inevitable [21]. As a solution to this problem, the PS-SMC algorithm is proposed as the simple solution that is easiest, quicker, and most effective.

Please cite this article in press as: Farhat M et al. A new maximum power point method based on a sliding mode approach for solar energy harvesting. Appl Energy (2016), http://dx.doi.org/10.1016/j.apenergy.2016.03.055

This paper presents a unique combination of a partial shading detector, voltage reference estimator and a sliding mode controller. This method is suitable to guarantee MPPT even under partial shadowed conditions. The originality of the method is in the usage of the voltage reference estimator and the partial shadow detection unit; this method supervises the MPPT voltage value continuously and is able to detect when the MPPT voltage is perturbed by the presence of PS. Once the PS is detected, an adjustment of the voltage value is triggered; the adjustment considers the voltage reference estimator output as an initial condition. The global MPP is calculated and the MPPT operation point is changed accordingly using a robust SMC. The important advantage of this method is its simplicity, since the partial shadow detection unit can be combined with any MPPT algorithm, such as the sliding mode controller, as is the case in the present paper. This method operates successfully even though a partial shadow arises. The effectiveness of the proposed method is confirmed by the obtained result.

The paper is structured as follows: a brief description of the considered PV model is presented in Section 2, while Section 3 deals with the explanation of the entire proposed MPPT method; a detailed analysis of the voltage reference generator and a sliding mode controller method is described. Section 4 is dedicated to the partial shadowing (PS) study and the description of the PS-SMC algorithm. Simulation results are carried out in Section 5. The effectiveness of the SMC MPPT is experimentally investigated in Section 6. Finally, some conclusions and future work are described in Section 7.

2. Photovoltaic energy conversion

2.1. PV generator model

One can substitute for a PV cell, an equivalent electric circuit that contains a power supply and a diode as shown in Fig. 2. Every PV generator is characterized by its maximum power point that is obtained in a defined voltage value, but due to the fact that this point is variable depending on the weather conditions; irradiation and temperature, creating a voltage reference estimator seems to be the best way in order to generate the right voltage value in any condition.

The power source produces the I_{ph} current which depends on impinging irradiation. Through the diode flows current I_d. The current I_c feeding the load is the difference between I_{ph} and I_d which is reduced by the resistance R_S. This last represents resistances of the cell and connection among cells [21,22].

The node law gives:

$$I_c = I_{ph} - I_d - I_{sh} \tag{1}$$

The current I_{ph} can be evaluated as:

$$I_{ph} = \frac{G}{G_{ref}}(I_{rs\_ref} + K_{SCT}(T_c - T_{c\_ref})) \tag{2}$$

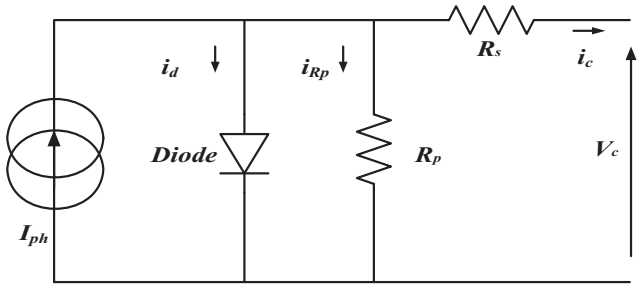

Fig. 2. Simplified PV cell equivalent circuit.

$$I_d = I_{rs}\left(\exp\frac{q(V_c + R_sI_c)}{\alpha kT} - 1\right) \tag{3}$$

$$I_{sh} = \frac{1}{R_p}(V_c + R_sI_c) \tag{4}$$

The reverse saturation current at reference temperature can be approximately obtained as:

$$I_{rs} = \frac{I_{rs\_ref}}{\exp\left[\frac{qV_{oc}}{n_s \cdot n \cdot \beta \cdot T_c}\right] - 1} \tag{5}$$

Finally, the cell current I_c can be given by:

$$I_c = I_{ph} - I_{rs}\left(\exp\frac{q(V_c + R_sI_c)}{\alpha kT} - 1\right) - \frac{1}{R_p}(V_c + R_sI_c) \tag{6}$$

The modeling of a PVG as given in Fig. 3 depends on N_S and N_p that are the total numbers of series and parallel modules respectively.

$$\begin{cases} I_p = N_pI_c \\ V_p = N_sn_sV_c \end{cases} \tag{7}$$

Finally the PVG current (I_p) can be given by,

$$I_p = N_pI_{ph} - N_pI_{rs}\left(\exp\frac{q}{\alpha kT}\left(\frac{V_p}{n_sN_s} + \frac{R_sI_P}{N_p}\right) - 1\right) - \frac{N_p}{R_p}\left(\frac{V_p}{n_sN_s} + \frac{R_sI_P}{N_p}\right) \tag{8}$$

The terms containing R_s and R_p parameters could be eliminated by simplification assumption $R_p \gg R_s$. Here the ideal model case is considered such as $R_s = 0$ and $R_p = \infty$.

$$I_p = N_pI_{ph} - N_pI_{rs}\left(\exp\frac{q}{n\beta T_c}\left(\frac{V_p}{n_sN_s}\right) - 1\right) \tag{9}$$

In this work, the ATERSA A55 PV manufactured module has been considered for simulation and practical validation purposes. This module has 36 series connected monocrystalline cells ($ns = 36$). The manufacturing specifications are given in Table 1.

Modules ATERSA A55 ($637 \times 527 \times 35$) are characterized as being professional panels. They are built with mono-crystalline silicon cells that guarantee power production. The performance of solar cells is normally evaluated under the standard test condition, the irradiance is normalized to 1000 W/m^2, and the cell temperature is defined as 25 °C.

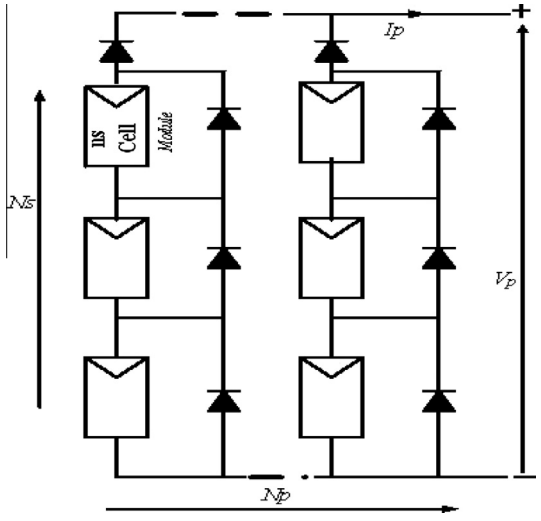

Fig. 3. A PVG group of modules; N_s numbers in series and N_p in parallel.

Please cite this article in press as: Farhat M et al. A new maximum power point method based on a sliding mode approach for solar energy harvesting. Appl Energy (2016), http://dx.doi.org/10.1016/j.apenergy.2016.03.055

Table 1
Specifications of the Atersa PV panel.

Cell type	Monocrystalline
Maximum power (W)	55
Open circuit voltage, V_{oc} (V)	20.5
Short circuit current I_{sc} (A)	3.7
Voltage, max power V_{MPP} (V)	16.2
Current, max power I_{MPP} (A)	3.4
Number of cells in series	36
Temp. coeff. of I_{sc} (mA/°C)	1.66
Temp. coeff. of V_{oc} (mV/°C)	−84.08

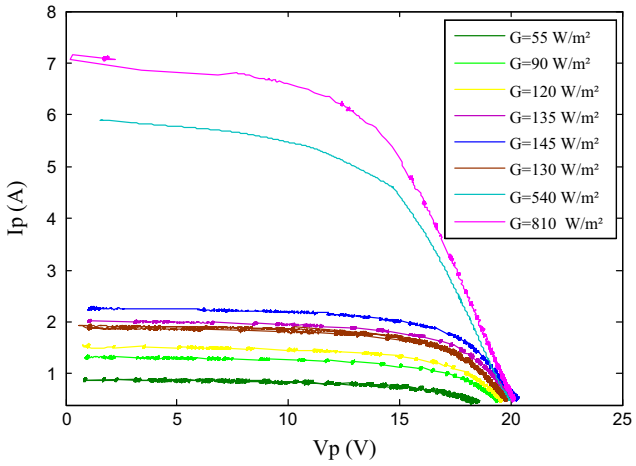

Fig. 4. *I–V* characteristics for different irradiations.

In order to increase the power, four modules are connected in parallel to form the PV panel that will be used in this paper. The extreme *I–V* nonlinear characteristics are shown in Fig. 4. These real characteristics are logged and plotted for different radiation values and an almost constant temperature.

2.2. Power boost converter

DC–DC converters are electronic devices used whenever there is a need to bring up or down a DC electrical voltage level to another. In this work, the Boost converter will hold the PVG maximum working point through a regulator called MPPT. Hence, the current PVG system efficiency is boosted. In order to step up the voltage, the operation switches an IGBT shown in Fig. 5 at a high commutation frequency with output voltage control by varying the switching duty cycle (D) [23,24]. Fig. 5 shows the circuit diagram of the converter and the load. The boost converter specifications are shown in Table 2. The converter is assumed to operate in a continuous conduction mode with two states based on the status of the switch [24].

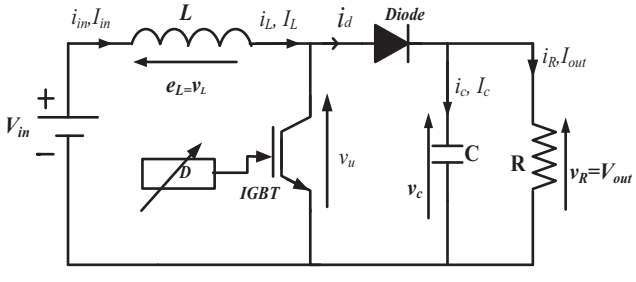

Fig. 5. Circuit diagram of the Boost converter.

Table 2
Boost converter parameters.

Schottky Diode	2× MURF1560GT	600 V, 15 A, 0.4 V at 10 A, 150 °C
IGBT	1× HGT40N60B3	600 V, 40 A, 1.5 V at 150 °C
L	6× PCV-2-564-08	560 μH, 7 A, 42 mΩ
C	2× TK Series	1500 μF, 250 V

Mode1: In the first state, the IGBT On, diode is Off. During this phase, the inductor is directly connected to the PVG and the diode is blocked. The load is then disconnected from the supply. The current in the inductance increases by storing magnetic energy. Considering that the variable state is:

$$x = \begin{pmatrix} i_L \\ v_R \end{pmatrix} = \begin{pmatrix} x_1 \\ x_2 \end{pmatrix}$$

$$\begin{cases} \dot{x} = A \cdot x + B \cdot u \\ y = E \cdot x + F \cdot u \end{cases} \quad (10)$$

With $E = [0\,1]$, $F = 0$, $u = v_{in}$, $y = v_{out}$.
The Kirchhoff's laws on the converter circuit yields:

$$\begin{cases} v_{in} = v_L = L\frac{di_L}{dt} = L\dot{x}_1 \\ v_{out} = v_c = v_R = x_2 \end{cases} \Rightarrow \begin{cases} \dot{x}_1 = \frac{1}{L} v_{in} \\ i_c = -i_R \Longleftrightarrow \dot{x}_2 = -\frac{1}{Rc} x_2 \end{cases} \quad (11)$$

With $A_1 = \begin{bmatrix} 0 & 0 \\ 0 & -\frac{1}{RC} \end{bmatrix}; B_1 = \begin{bmatrix} \frac{1}{L} \\ 0 \end{bmatrix}$

Mode2: IGBT is Off; diode is ON: The inductor emf is added to that of the PVG. The current flows through the inductor, the capacitor, the diode and the load. The result is an energy transfer stored in the inductor to the capacitor.

$$\begin{cases} v_{in} = v_L + v_{out} \\ i_c = i_L - i_R \end{cases} \Rightarrow \begin{cases} \dot{x}_1 = -\frac{1}{L} x_2 + \frac{1}{L} v_{in} \\ \dot{x}_2 = \frac{1}{C} x_1 - \frac{1}{RC} x_2 \end{cases} \quad (12)$$

With $A_2 = \begin{bmatrix} 0 & -\frac{1}{L} \\ \frac{1}{C} & -\frac{1}{RC} \end{bmatrix}$; $B_2 = \begin{bmatrix} \frac{1}{L} \\ 0 \end{bmatrix}$

As a result

$$\begin{cases} A = DA_1 + (1-D)A_2 \\ B = DB_1 + (1-D)B_2 \end{cases} \quad (13)$$

$$A = \begin{bmatrix} 0 & \frac{D-1}{L} \\ \frac{1-D}{C} & -\frac{1}{RC} \end{bmatrix}; \; B = \begin{bmatrix} \frac{1}{L} \\ 0 \end{bmatrix}$$

The steady-state solution of the converter in continuous conducting mode is therefore [25]

$$G = \frac{y}{u} = \frac{V_{out}}{V_{in}} = E \cdot (-A)^{-1} B + F \quad (14)$$

The steady-state solution is equivalent to

$$V_{out} = \frac{1}{1-D} V_{in} \quad (15)$$

Based on the assumption where $P_{in} = P_{out}$ it can be deduced that

$$R_{pv} = (1-D)^2 R_{out} \quad (16)$$

where R_{pv} is the equivalent resistance connected to the PV panel [26].

3. MPPT control

The Maximum Power Point Tracking (MPPT) control is a fundamental phase in order to obtain a good performance in a PVG system. Usually, the principle of this MPPT is based on adapting or varying the converter duty cycle (D) to finally bring the PVG working in its MPP. The Perturb & Observe is the most common

method, however, it presents a lot of drawbacks. As a solution to overcome these drawbacks, a MPPT new control method which is based on SMC is proposed in this section.

3.1. P&O algorithm principle

Due to its simplicity, the P&O algorithm is the most popular [27]. The principle of this controller is to provoke perturbation by acting on (decrease or increase) the PWM duty cycle command and observing the output PVG power reaction. If the present power $P(k)$ is greater than the previous computed one $P(K-1)$, then the perturbation direction is maintained. Otherwise, it is reversed [28].

The P&O algorithm can be detailed as follows:

- When the ratio $\Delta P/\Delta V$ is positive, the voltage must be increased, this yields

$$D(K) = D(K-1) + \Delta D, (\Delta D : crisp\ value)$$

- When the ratio $\Delta P/\Delta V$ is negative, the voltage must be decreased through

$$D((k) = D(k-1) - \Delta D.$$

The ΔD crisp value is chosen by trial and tests in simulation. If the crisp value ΔD is very large or very small, then we may lose information. Despite the fact that the P&O algorithm is easy to implement, it principally has the following problems [1,29]:

- The PV system will always operate in an oscillating mode.
- The PV system may fail to track the maximum power point.

3.2. Sliding mode controller

The SMC-MPPT algorithm is divided into two steps. The first is to estimate the actual reference voltage (V_{MPP}) value at which the system will reach its maximum power. The second is the SMC PVG voltage regulation at the V_{MPP} voltage value. These steps lead to a PVG MPP working point.

The main role of this controller is to generate a command using a voltage reference (V_{ref}) in order to force the system to work at the maximum power point (MPP). The main novelty in this method is to define the input of the controller as: $Vp - V^*_{MPP}$. This input can be easily calculated and based on the bijectivity principle between V_{MPP} and P_{MPP}. So if the system will work at the V_{MPP}, the maximum of power will be obtained (P_{MPP}).

Step1: voltage reference estimator

Authors in [30] calculate the voltage V_{MPP} value such as, $V_{MPP} = K_v * V_{oc}$, with V_{oc} is the open circuit, or by directly reading and sending V_{MPP} to the regulator [31]. This last requires basically a direct knowledge of the V_{oc} or V_{MPP} values. Generally, users of this method draw the PV characteristics and then feed the target values to the MPPT regulator. This method poorly tracks the V_{MPP} input value that actually changes according to the temperature and depends on the irradiation values as shown in Fig. 6. Fig. 6 shows that for almost constant temperature and different irradiation values, the maximum power (P_{MPP}) is obtained for different voltage values (V_{MPP}). By joining the different MPP obtained for different irradiation values, we can construct the red curve that for a given (P_{MPP}) value indicates the corresponding V_{MPP}. Therefore, this red curve can be used as a MPP voltage reference estimator constructed using a fitting function F with $V_{MPP} = F(P)$.

Fig. 7 explains that for any state, after several iterations (projection), the system will be forced to work with the desired voltage V_{MPP} and hence meets the MPP. For example, assuming that the PV system is working in an operating point 'P1', after projection

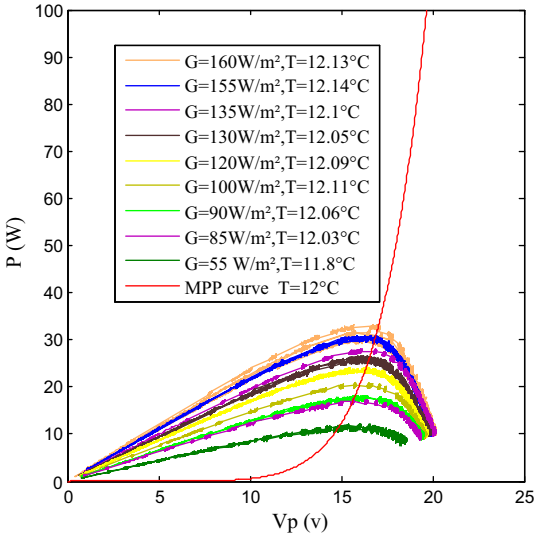

Fig. 6. Real P–V characteristics for different irradiations at almost constant temperature.

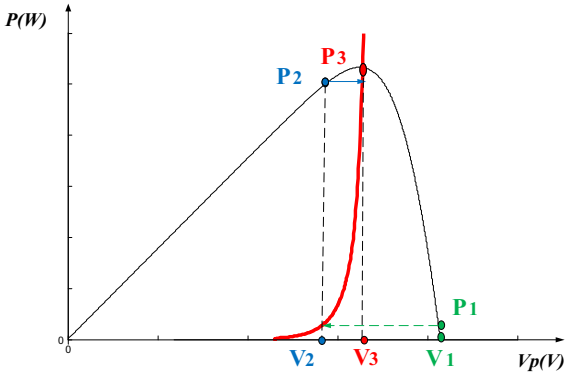

Fig. 7. P–V characteristics at fixed temperature value of 25 °C.

using the reference voltage curve, the reference voltage changes from "V1" to "V2" and consequently the operating point of the PV system will change its position to 'P2'. Using the same principle, the 'P2' will be projected again on the reference curve, and changes its position until the operating point reaches the MPP as shown in Fig. 7 where finally P3 = P_{MPP}. As a result, the constructed red curve can be used as a MPP reference voltage estimator. The main and direct advantage of this approach is that we can overcome the usually required solar radiation sensor.

Fig. 8 shows the PVG characteristics for different temperature values such as 12 and 37 °C. In this figure, the V_{MPP} values are lying between 11.96 V and 16.99 V, which can be considered as a big range. As a result the V_{MPP} is directly connected to the temperature values. As a consequence, one should consider an independent reference voltage curve for each temperature value. In the next part of this paper, the voltage reference (V_{MPP}) estimator is constructed to generate the V_{MPP} for actual temperature values.

Since the PV optimal or reference voltage value also depends on the temperature, it is necessary to build an estimator that only considers the temperature values. Fig. 9 presents the curve of the MPP ($V_{MPP} = F(P_{MPP})$) power to voltage characteristics for the different couples (V_{MPP}, P_{MPP}) obtained for different conditions. These couples have been collected from real characteristics. All points (V_{MPP} P, T) are interpolated to obtain the function $V_{MPP} = F(P, T)$ which provides the voltage value at the MPP for any power value

Please cite this article in press as: Farhat M et al. A new maximum power point method based on a sliding mode approach for solar energy harvesting. Appl Energy (2016), http://dx.doi.org/10.1016/j.apenergy.2016.03.055

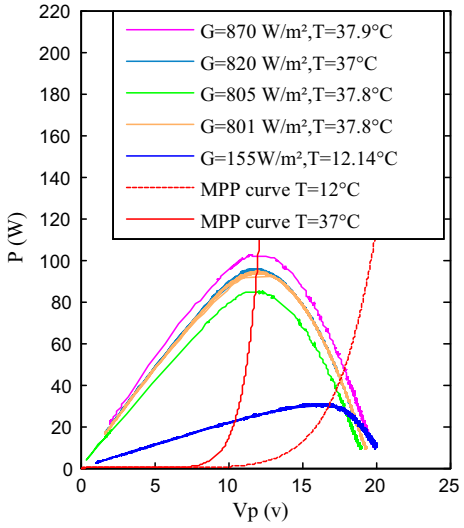

Fig. 8. Real *P–V* characteristics for different irradiation and temperature values.

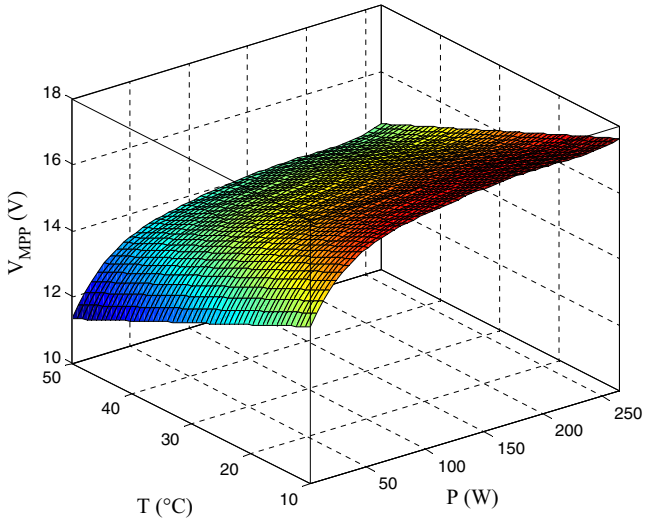

Fig. 10. Surface power–temperature–voltage characteristic of MPP.

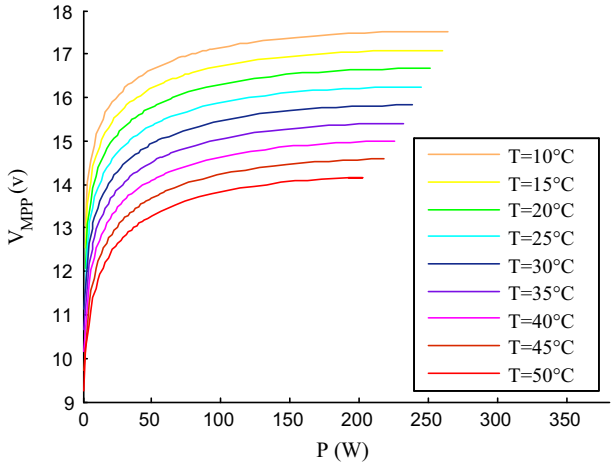

Fig. 9. Optimal power–voltage characteristics for different temperature values.

at a given temperature. Several tests have been performed using different types of functions [32,33]. Finally, it is deduced that the following function provides the better interpolation for the Atersa model. The constructed function is denoted as:

$$\begin{aligned} V_{MPP} &= F(X,Y) \\ &= p_{00} + p_{10} * X + p_{01} * Y + p_{20} * X^2 + p_{11} * X * Y + p_{30} * X^3 \\ &\quad + p_{21} * X^2 * Y + p_{40} * X^4 + p_{31} * X^3 * Y + p_{50} * X^5 \\ &\quad + p_{41} * X^4 * Y \end{aligned} \tag{17}$$

$With\ X = (P - meanX)/stdX$ and $Y = (T - meanY)/stdY$

$meanX = 73.38, stdx = 67.38; meanY = 29.7, stdY = 13.05$

$p_{00} = 15.29 \quad p_{10} = 0.6488 \quad p_{01} = -1.09$

$p_{20} = -0.5132 \quad p_{11} = 0.01793 \quad p_{30} = 0.4582$

$p_{21} = -0.01153 \quad p_{40} = -0.2286 \quad p_{31} = -0.001497$

$p_{50} = 0.04033 \quad p_{41} = 0.001746$

Fig. 10 shows the surface that provides the reference voltage for different power and temperature values.

Step 2: SMC

After the estimation of V_{MPP}, the implemented SMC is used to drive the regulation element in such a way to reduce the actual voltage error between the acquired PVG voltage and the target V_{MPP}. The boost converter is forced to bring up the PVG to operate at the desired reference voltage value (V_{ref}) and therefore at the maximum power working point.

$$S = e = V_p - V_{ref} \tag{18}$$

$$u = \frac{1}{2}(1 + Sign(S)) \tag{19}$$

$$u = \begin{cases} 1 & S > 0 \\ 0 & S < 0 \end{cases} \tag{20}$$

Stability demonstration:

The stability can be analyzed based on the Lyapunov theory. A positive definite function V is defined as:

$$V = \frac{1}{2}S^2 > 0 \tag{21}$$

Whose time derivative is: $\dot{V} = S\frac{dS}{dt} = S\dot{S}$.

Considering $\begin{cases} S = e = V_p - V^*_{MPP} \\ \dot{S} = \dot{e} = \dot{V}p \end{cases}$.

Next, based on the principle of Lyapunov, it is demonstrated that S reaches the state $S = 0$. Therefore the system reaches the desired voltage value V_{MPP}, and thus reaches the point of maximum power.

When S > 0

The switch will be open; this implies that the duty cycle will increase. From the boost converter model Eq. (16) we have, $R_{pv} = (1 - D)^2 R_{out}$ and using this equation, we can observe that:

– If the duty cycle D increases, then R_{pv} decreases, so based on the PV dynamic given by the *I–V* characteristic shown in Fig. 11, the I_p will increase and V_p will decrease equivalently from Eq. (9). It can be deduced that when the voltage (V_p) increases/decrees, the current (I_p) decreases/increases.

So, as a result in this case, this implies $\dot{V}p < 0$ and $\dot{S} < 0$

Finally, $S\dot{S} < 0$.

When S < 0, Using the same method.

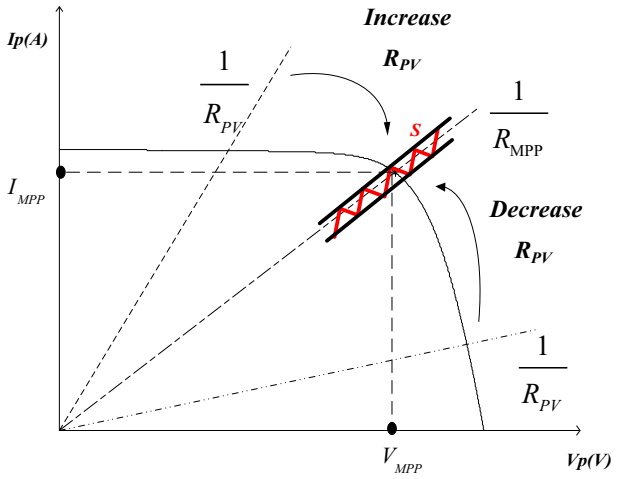

Fig. 11. *I–V* characteristics and MPPT process.

The switch will be close, this implies that the duty cycle will decrease. If the duty cycle D decreases, then $R_{pv} = (1-D)^2 R_{out}$ increases. Therefore, based on the PV dynamic given by the *I–V* characteristic shown in Fig. 11, the I_p will decrease and V_p increases equivalently from Eq. (9). It can be deduced that, when the voltage (V_p) decreases/increases the current (I_p) will increase/decrease, so:

If the resistance connected to the PV panel increases then (V_p) increases and (I_p) decreases, this implies that:

$\dot{V}p > 0$ and $\dot{S} > 0$

So $S\dot{S} < 0$

Finally, using the Lyapunov stability theory it can be concluded that S reaches the state $S = 0$, meaning that the system reaches the desired voltage value V_{MPP} and hence the converges to the point of maximum power.

4. Partial shadowing of photovoltaic arrays (PVG)

A number of series/parallel connected PV modules are used to construct a PVG for a desired voltage and current level as previously shown in Fig. 3. The performance of the series connected string of the solar cells is unfortunately affected if all its cells are not equally illuminated (partially shaded) [34]. Fig. 12 shows the characteristics of the PVG in cases of shadow presence or no shadow presence.

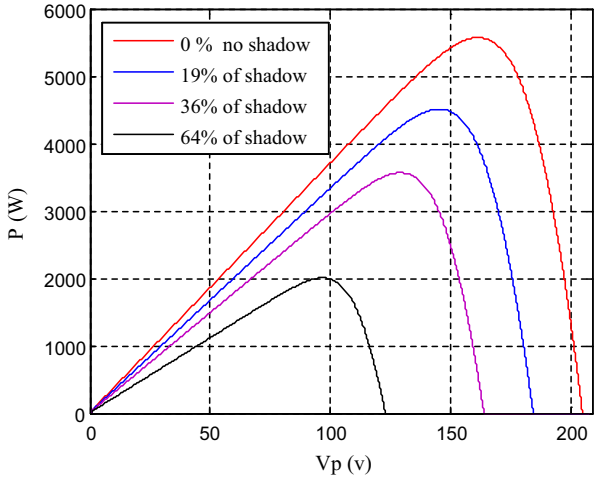

Fig. 12. *P–V* Characteristics under constant irradiation (1000 W/m^2) and temperature (25 °C) values.

Partial shadow (PS) is a common reason of power loss in a photovoltaic application. This loss of efficiency can occurs in many ways. Depending on the object causing the shading, it could only be seasonal, or for a few hours each day, resulting in obviously mysterious fluctuations in the power as shown in Fig. 12 [35].

This paper proposes an additional algorithm to be added after the voltage reference estimator and before the SMC controller in order to correctly track the MPP against PS disturbance occurring. This work proposes a system based on a simple partial shadow detection method that will be trigged only when PS is detected; in order to check the presence of a PS, this algorithm makes a test every one second; this is accomplished through the test of the power value. As a result, when the power decreases by 10% the correction action will be trigged. This algorithm is called PS-SMC. The flowchart of the PS-SMC concept is shown in Fig. 13. It is divided in three main parts:

- Generating the optimal voltage V_{MPP} under ordinary conditions (no partial shadowing), using the voltage reference estimator.
- Detection of the partial shadow and search for the new optimal voltage.
- Forcing the system to operate with the optimal voltage using the SMC.

In this algorithm, temperature and current voltage sensors are required for the voltage reference estimator. The same current and voltage will be later used for the calculation of the power values.

First, the voltage reference estimator generates the V_{MMP}. After receiving this last value, this algorithm makes a test every period of one second in order to test the existing shadow by detecting a decrease in the power values. In the case of no-existence of power loss, the current V_{MMP} is directly given as an input for the SMC. Otherwise if it detects a decrease of 10% in power quantities (if $\Delta P < 10\%$), the search for the new optimal voltage (new MPP) will begin. This algorithm will start the search from the V_{MMP} to the

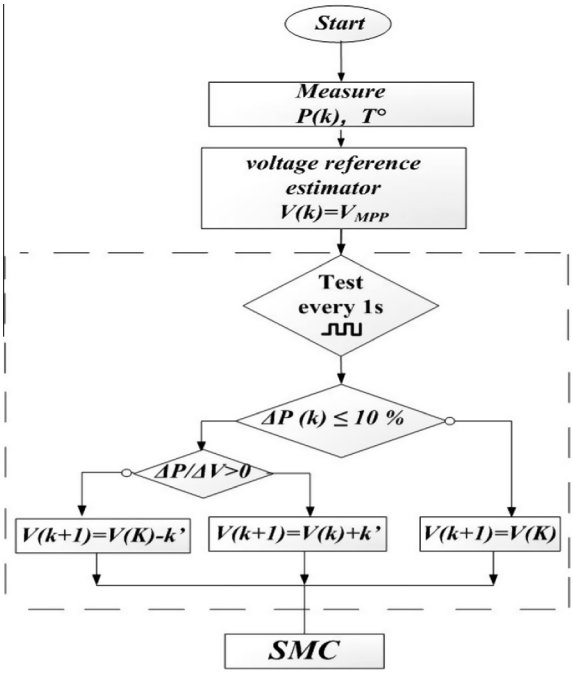

Fig. 13. PS-SMC algorithm flowchart.

Please cite this article in press as: Farhat M et al. A new maximum power point method based on a sliding mode approach for solar energy harvesting. Appl Energy (2016), http://dx.doi.org/10.1016/j.apenergy.2016.03.055

optimal voltage of the PVG under ordinary conditions. This last voltage is generated by the used voltage reference estimator. In order to minimize the $\Delta P/\Delta V$ ratio value [5,29,36], and starting from the actual V_{MMP}, the voltage is decreased or increased according to the sign of $\Delta P/\Delta V$ with k' as a constant of the PS-SMC. Finally, the system operates in the new optimal voltage via the SMC.

5. Simulation results

In this section, the PV system global control scheme, shown in Fig. 13, is implemented. To highlight the proposed scheme's best performances, the MPPT PS-SMC controller must act on the converter duty cycle yielding an optimal load voltage in a given condition. In the simulation, the condition of 1000 W/m^2 and 500 W/m^2 are carried out.

Fig. 14 presents the *I–V* and *P–V* characteristic at fixed temperature and different irradiation values (500 and 1000 W/m^2). Fig. 14 presents also the panel characteristic under a partial shadow, and the MPP's characteristics of each case are presented in Table 3.

The used PV panel contains 10 modules connected in series ($Ns = 10$) and 10 modules connected in parallel ($Np = 10$) as shown in Fig. 15.

The PS-SMC, with optimal voltage reference, is compared to P&O algorithm. Both controllers are tested over external and internal variation. The system is tested over a sudden step irradiation and load changes as shown respectively in Figs. 16 and 17. This action is used to prove the controller robustness and the ability to keep extracting the maximum power within this abrupt variation. In order to test the PS-SMC robustness against PS the system will suffer 19% of partial shadowing from 1 to 3 s as shown in Fig. 18.

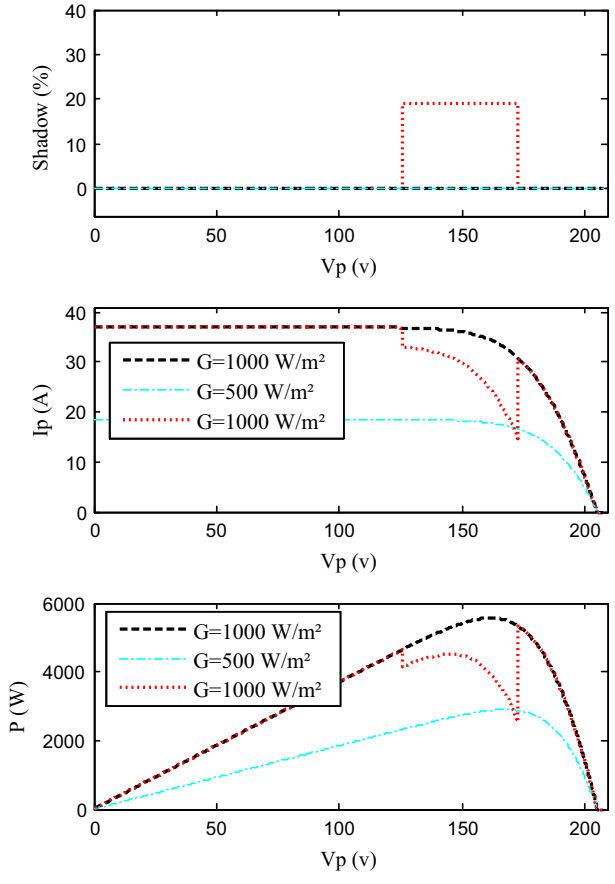

Fig. 14. *P–V* Characteristics under PS appliance.

Table 3
MPP voltage and power.

Condition	Voltage (V)	Power (W)
$G = 1000$ W/m^2, no shadow	161.8257	5.5700e+03
$G = 1000$ W/m^2, shadow	145.6400	4.5117e+03
$G = 500$ W/m^2, no shadow	167.7343	2.9029e+03

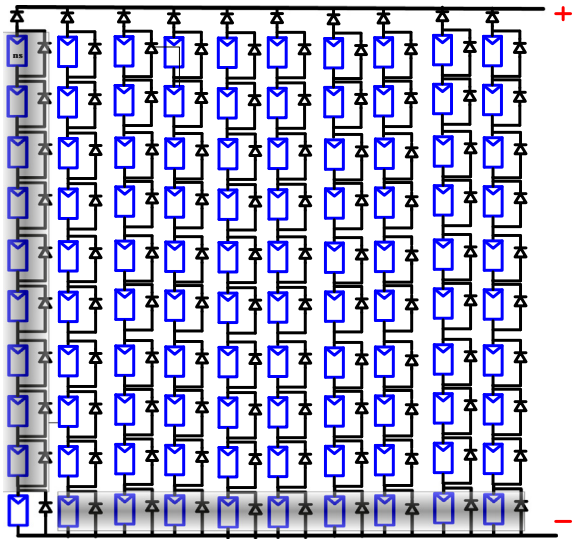

Fig. 15. PV array configuration.

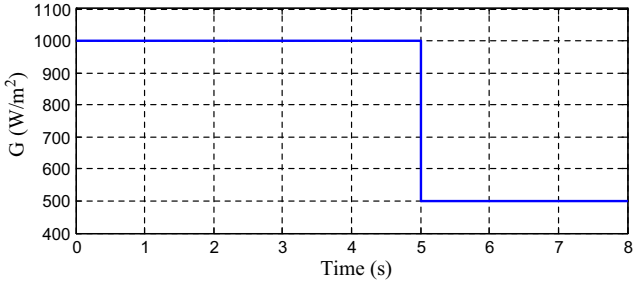

Fig. 16. Irradiation abrupt variation.

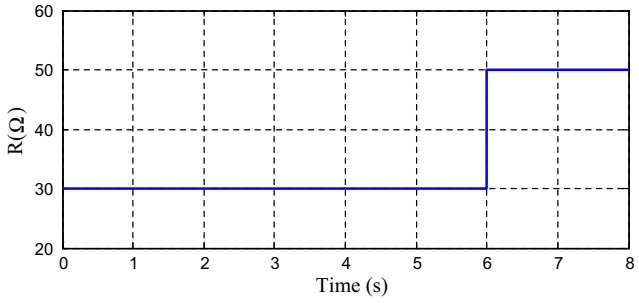

Fig. 17. Load abrupt variation.

The results shown in Fig. 19 demonstrate the obtained results of P&O and the PS-SMC tracker's stability. The PS-SMC has very short response time and overshoots. Moreover, PS-SMC presents a reduced oscillation signal in the MPP compared with the P&O one.

Fig. 20 presents the duty cycle signal delivered by the P&O algorithm, which will be used with a reference saw signal to generate a PWM IGBT drive signal. Fig. 20 also shows the direct PWM signal

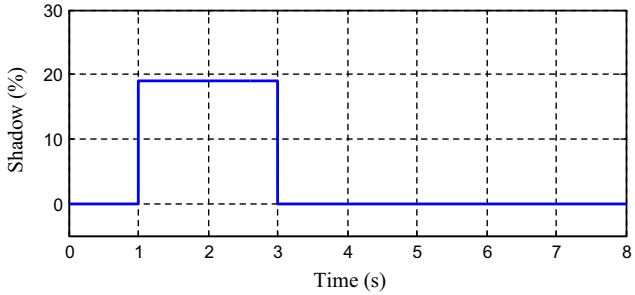

Fig. 18. Partial shadow abrupt variation.

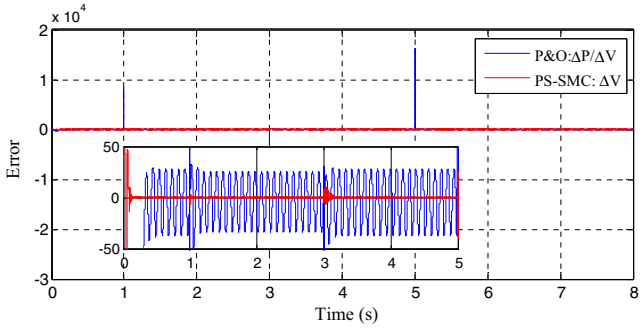

Fig. 19. Controllers performances.

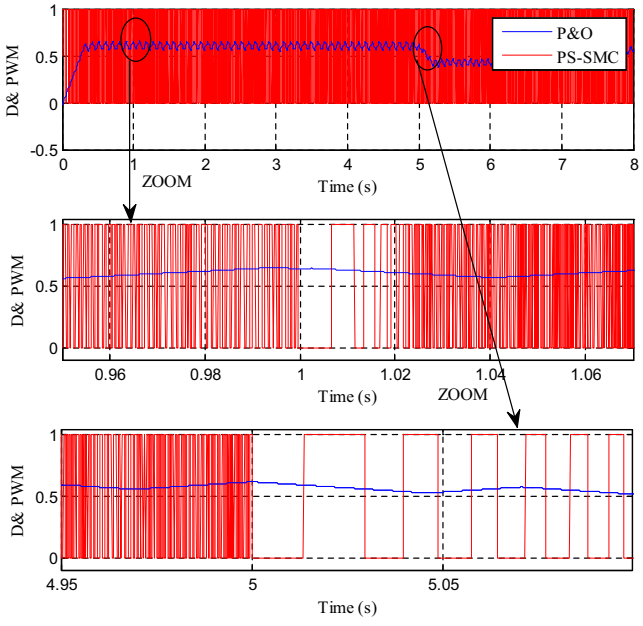

Fig. 20. Controllers signal output.

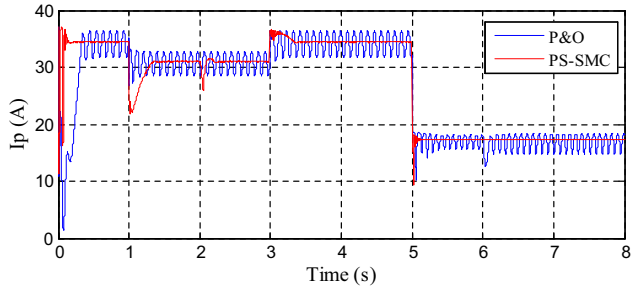

Fig. 21. PVG current behavior.

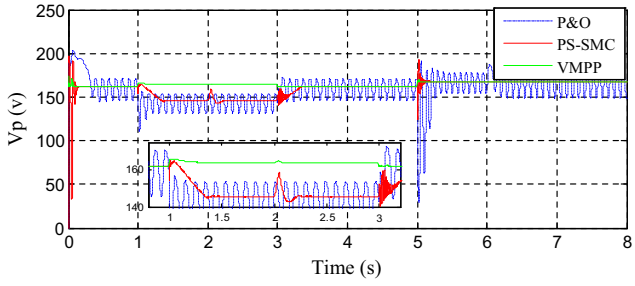

Fig. 22. PVG voltage behavior.

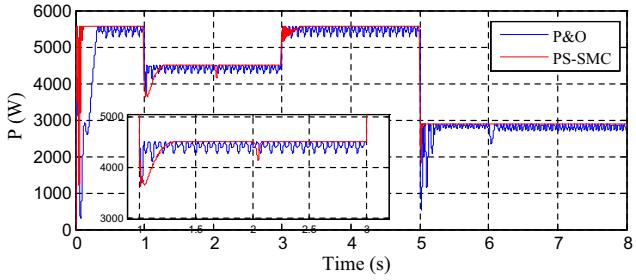

Fig. 23. PVG power.

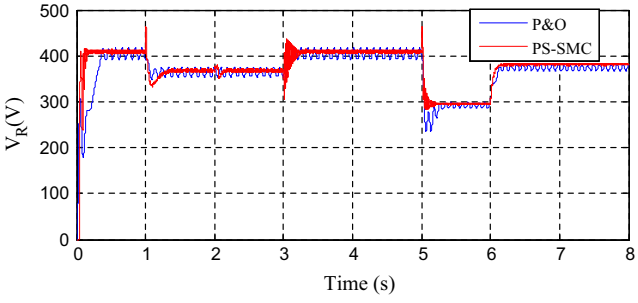

Fig. 24. The load feeding voltage.

generated by the PS-SMC. This has the benefit of avoiding the use of a PWM commutation signal (saw signal). It permits directly constructing the PWM output signal toward the IGBT Gate. In Fig. 20 close up (at second 1 and 5), it is clear that the PWM frequency is affected by the condition changes.

Figs. 21–23 shows the PVG current, voltage and power respectively. As observed in Fig. 23, the P&O algorithm tracks the new MPP yet always generates an oscillating signal around the optimal power value.

Fig. 22 shows the output of the voltage reference estimator (V_{MPP}); when the PV system is under partial shadow, this voltage doesn't correspond to the voltage at the correct MPP. In this case, the PS-SMC acts in order to adequately modify the MPP reference voltage using the algorithm presented in Fig. 13.

It is clear that in the magnified portion of second 2 there is a small perturbation. This perturbation is caused by the PS-SMC test (every second in case of shadow detection) to verify that there is still a partial shadow.

Please cite this article in press as: Farhat M et al. A new maximum power point method based on a sliding mode approach for solar energy harvesting. Appl Energy (2016), http://dx.doi.org/10.1016/j.apenergy.2016.03.055

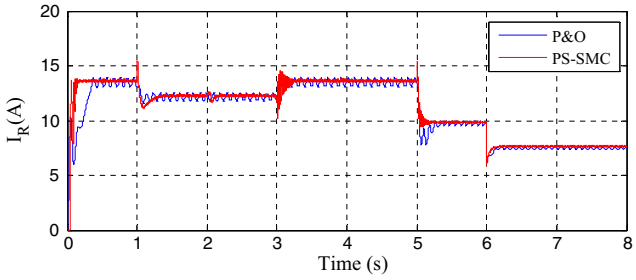

Fig. 25. Load current.

Table 4
Comparison of MPPT techniques.

MPPT algorithm	P&O	SMC
Parameters knowledge	Not necessary	Not necessary
Complexity	Low	Low
Convergence speed	Medium	Rapid
Precision	Low	High
Efficiency	Low	High

At second 5, the irradiation changes, the MPP also changes its position, and so the controllers act in order to track the new MPP. Figs. 22 and 23 show that in spite of the load change in second 6, the operation point of the PV remains constant in the MPP due to the robustness of the controllers. It is noteworthy that the rate of oscillation depends on the controller robustness.

Figs. 24 and 25 show the load voltage and current.

The obtained simulation results show that both systems using different controllers present a good maximum power tracking, however, the SMC controller presents less oscillations and faster tracking in its response. A comparison of MPPT techniques is shown in Table 4.

The P&O algorithm is a classic and simple algorithm. This algorithm depends highly on initial conditions and usually presents undesirable oscillations around the optimal value. The major drawbacks of this algorithm are its bad behavior in a sudden change of irradiation (clouds). Moreover, if the crisp value is very large or very small, then we may lose information. Despite the fact that P&O algorithm is easy to implement, the PV system always operates in an oscillating mode and may fail to track the maximum power point, as result the system operates in current or voltage zones, because in these mentioned areas the power variation is very low [37–40]. The algorithm based on a sliding mode control is a robust and efficient algorithm, [41]. Indeed, this algorithm works at the optimum point without oscillations. Furthermore, it is characterized by a good behavior in transient state.

This work is focusing on SMC as an MPPT. The main purpose of this paper is to add a voltage reference estimator that generates the V_{MMP} in ordinary conditions and also add a PS algorithm that detects shadow and generates the adequate voltage value. In order to gain time, The PS algorithm starts the research of the new V_{MPP} from the last value given by the voltage reference estimator. Later, the adequate voltage will be considered as an input for the SMC controller that guarantees the system maximum efficiency and stability. Simulations were performed while rapidly changing shading, load and irradiation disturbances were applied, and the obtained results show that both systems using different controllers present a good maximum power tracking. However, the PS-SMC controllers present lesser oscillations, faster tracking in response and more stability. Moreover, the PS-SMC algorithm has been proved to be effective and sensitive to existing shading.

In order to prove the sliding mode controller's efficiency, a real implementation has been applied in the next section.

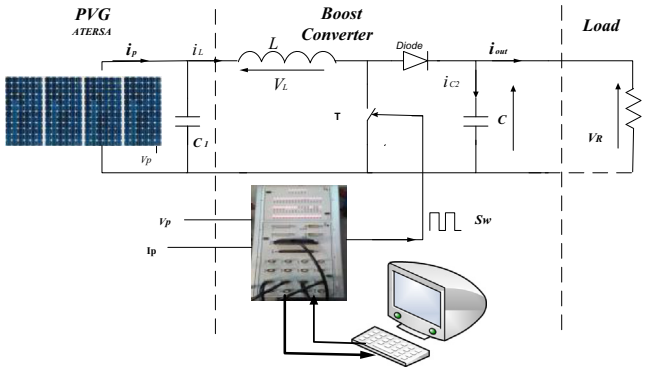

Fig. 26. The block diagram of the hardware stage.

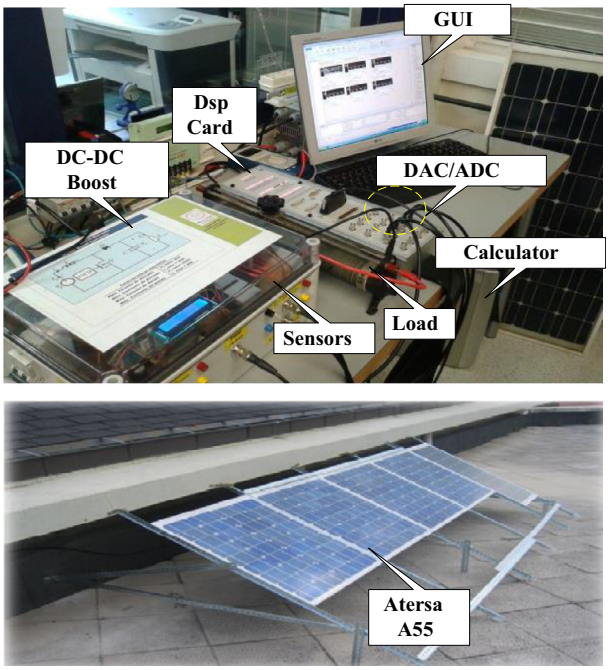

Fig. 27. Photo of the system hardware setup.

6. Practical experiment

In this section, a dSPACE controller board was used as central control platform. It enables the linkage between the MATLAB/SIMULINK and the real hardware platform. This is done by introducing the dSPACE 1104 with its RTI environment and interfaces [42].

In this experiment, the implementation of the MPPT controller is employed by using the dSPACE DS1104 real-time control platform. Fig. 26 shows the block diagram of the hardware setup while Fig. 27 is a photo of the hardware used for the MPPT-PV system. In the hardware system, four (4) ATERSA A55 modules are connected to the DC–DC boost converter that feeds a resistive load.

The data acquisition and the control system are implemented using dSPACE software and digital signal processor card on a PC. The acquired measures come directly from the sensors mounted in the boost converter. Fig. 28 shows The MPPT control which is constructed on MATLAB/SIMULINK.

The PV voltage and current are applied to the MPPT algorithm to generate the required duty cycle. The output signal of the MPPT algorithm is then applied to the DS1104SL DSP PWM block which is used to generate the required switching signal.

Please cite this article in press as: Farhat M et al. A new maximum power point method based on a sliding mode approach for solar energy harvesting. Appl Energy (2016), http://dx.doi.org/10.1016/j.apenergy.2016.03.055

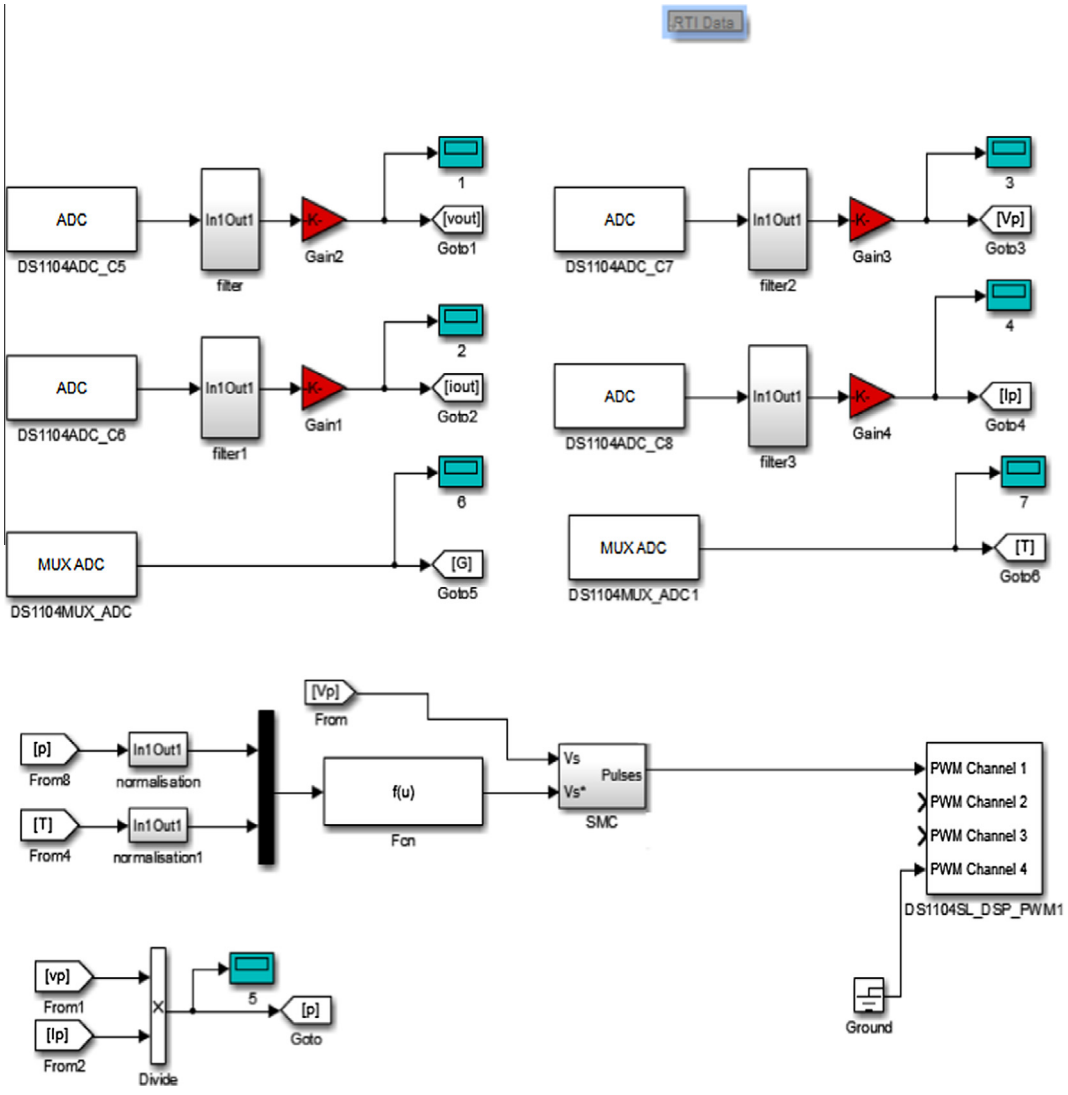

Fig. 28. MPPT SIMULINK model implemented in DSPACE-RTI.

To prove the performance of the proposed MPPT methods, the controllers are experimentally implemented by using the DSPACE data acquisition system. In order to start real-time MPP tracking of the PV generator, the SIMULINK MPPT control block must be downloaded to the DSPACE board to generate C code of the MPPT control block. All the obtained results in the next section were taken in Vitoria-Gasteiz, Spain at 9.46 am and the temperature cell is equal to 11.08 °C.

In order to start a new real-time experience, the block presented in Fig. 28 must be downloaded to the dSPACE board to generate the new C code. However, before starting the tracking operation we had interest: first in localizing the operation point of the system without control by sending a constant command equal to zero ($D = 0$) to the DS1104SL DSP PWM, and second, varying the load from 0.1 Ω to 47.2 Ω in order to get the real PVG characteristics.

Fig. 29 shows the ATERSA *P–V* and *I–V* characteristics respectively and also the operating point of a resistive load ($R \approx 27.1\ \Omega$) coupled to the PVG when the duty cycle is zero (that is, without any control). From the previous figures it is easy to see that the operating point of the resistive load is too far from the maximum power point. As explained in Fig. 11, by adding the SMC we will try to make the system work in the MPP. In this point an optimal power equal to 23.7 W shall be obtained.

The *P–V* characteristics shown in Fig. 29 demonstrate that the MPP is characterized by a voltage value equal to 16.36 and power value equal to 23.73. The PVG real operation point is showed in Table 5.

After recording the data to draw the characteristics, the SMC MPPT is added in the next set of results in order to improve the efficiency of the system and ensure a higher performance.

In order to initiate the real-time MPP tracking of the PV generator, the SIMULINK MPPT control block is downloaded again to the dSPACE board to generate the new C code of the MPPT control block. It should be noted that this operation needs some time. Therefore, for this new experiment a new PV characteristic that could be a little bit different from the PV characteristic drawn in the previous experiment due to the small changes in the radiation value.

In this actual experiment, the proposed SMC is analyzed in order to show its real performance. At a time ≈ 10.7 s we change the load manually in order to test the robustness of the controller; the approximate value of resistance is shown in Fig. 30.

Fig. 31 shows the irradiation values during recording that is almost equal to 120 W/m^2.

Please cite this article in press as: Farhat M et al. A new maximum power point method based on a sliding mode approach for solar energy harvesting. Appl Energy (2016), http://dx.doi.org/10.1016/j.apenergy.2016.03.055

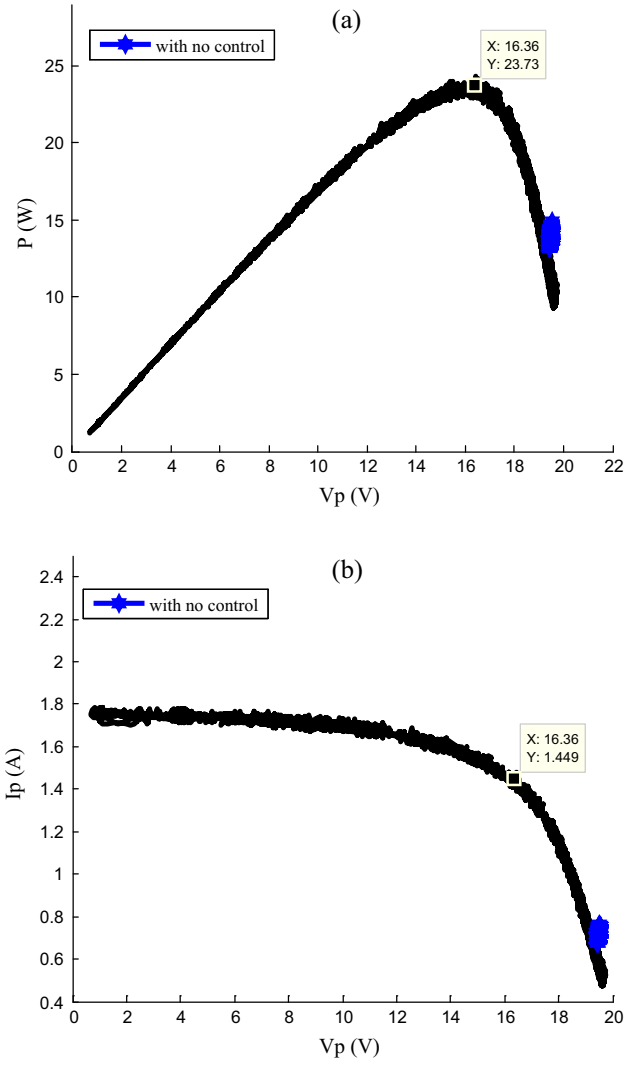

Fig. 29. Practical characteristics: (a) *P–V* and (b) *I–V* curves.

Table 5
PVG real operation point.

Condition	Voltage (V)	Power (W)
With SMC	16.36	23.73
With no control	19.42	13.23

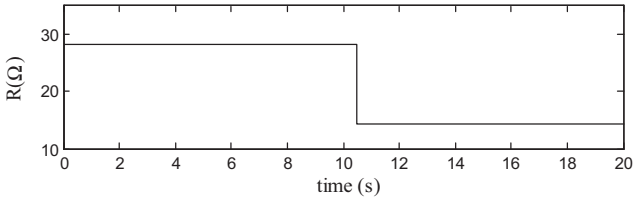

Fig. 30. Approximation of load profile.

Fig. 32 shows the controller performance; it is clear in this figure that the error controller is zero, which proves the system stability. Fig. 33 shows the operation point of the system during recording and varying the load value. This operation point consists of the voltage and power values. The operation point using SMC remains constant even with the load variation, proving the robustness of the proposed controller.

It is clearly shown in Fig. 33 that the PV system is operating with a voltage value equal to 16.36 and power value equal to 23.73. These values are the values presented previously in the *P–V* curve shown in Fig. 29 and Table 5. These matching values prove the success of the proposed algorithm to track the MPP.

Finally, Fig. 34 shows the load voltage and the current, respectively.

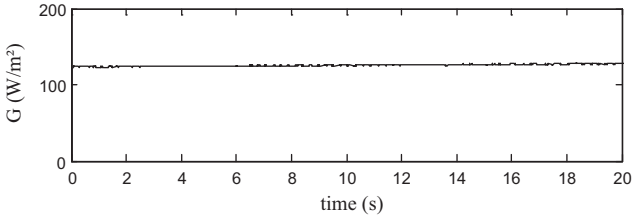

Fig. 31. Irradiation.

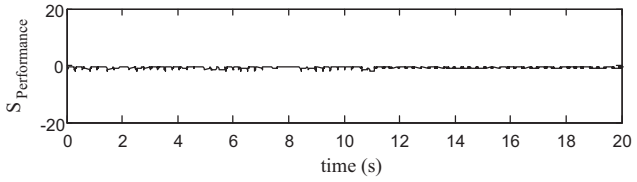

Fig. 32. Controller performance.

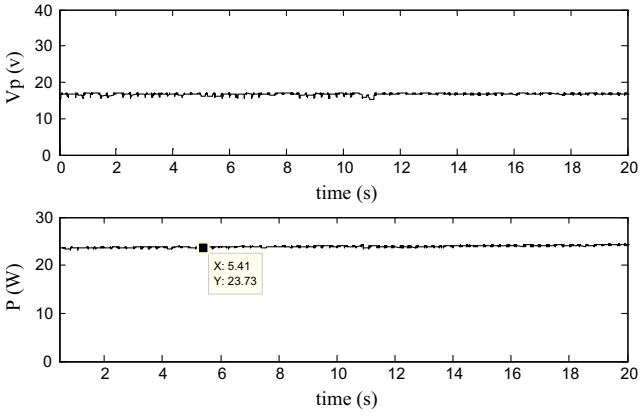

Fig. 33. PVG voltage (V_p) and power (P).

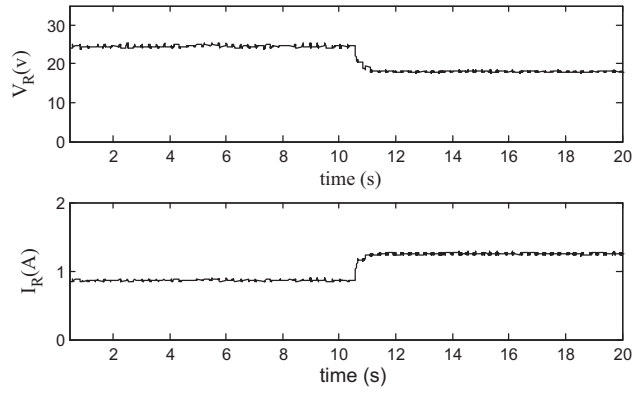

Fig. 34. Load voltage (V_R) and current (I_R).

From Fig. 33 it is easy to see that the system is operating with an average power equal to 23 W. This value corresponds to the point of the maximum power shown in Fig. 29. This power remains constant under load variation. Therefore, this figure shows the proposed SMC's tracking efficiency and robustness over that of the real PV system.

It should be noted that unlike the simulation work, the practical results present some noise in the signal as is usual because of the delay in the control signal, variation in the irradiation during recording time, and also parasite signals that come from the system component. At this point, it should be noted that with the use of the P&O control in this real PV system, the results oscillate too much and may even not attain the optimization goal as explained before.

The effectiveness of the PV system using SMC is clear in this paper, as well as its success to operate in the area of maximum power zone as shown in Fig. 35. Based on the tracking explanation in Section 3 and the description of Fig. 11, we can say that the SMC succeed in decreasing the load seen by the ATERSA panel in order to consume its maximum power. The SMC MPPT controller brings up the PVG performances as depicted in the PVG output tracking curves. The conclusions of Fig. 35 confirm that the output power harvested by the proposed MPPT method is the maximum power that can be generated from the PVG. This can be clearly seen through the SMC tracking power. The power rate benefits and the overall system performances are improved. The SMC MPPT controller improves the PVG performances seen in the PVG output tracking curves as compared to the no-control case. The obtained results confirm that the power rate is improved by 55%.

The SMC guarantees a huge gain in the generated power amount and thus the proposed design will find extensive applications in real life for instance, it would be very effective in a standalone photovoltaic water pumping system because the quantity of pumped water is relative to the amount of harvested PV energy [5]. This new algorithm is simple and can be safely implemented in real time digital applications.

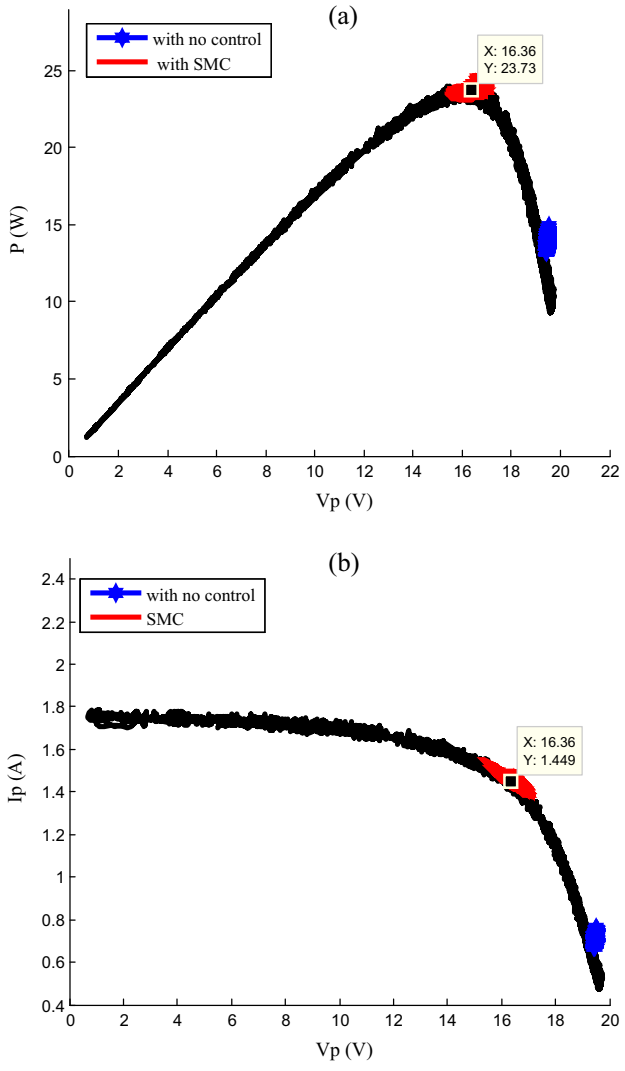

Fig. 35. Characteristics with MPPT drives: (a) *P–V* and (b) *I–V* curves.

7. Conclusion

A PVG system feeding a passive load type through a Boost converter is studied through simulation tests and practical implementation. To improve the system efficiency and performance, a MPPT DC–DC converter driven is synthesized based on the sliding mode theory. The stability of the proposed SMC-MPPT system is verified using the Lyapunov theory.

To perform an accurate and rapid SMC-MPP tracker, a simple and reliable estimator was constructed using only temperature and power sensors. This estimator generates the V_{MPP} according to simultaneous temperature and irradiation variations. It is dressed in an analytical form to be easy to implement. The proposed MPPT algorithm ensures robustness and high tracking performance. To compensate and overcome the PVG shadowing effects and drawbacks, a new algorithm is proposed PS-SMC. Many tests were performed in an extensive simulation work to verify the robustness and the high performance of the proposed PS-SMC algorithm against partial shadow, load profile, and irradiation variations. Obtained results were presented and discussed. A practical implementation work was performed yielding a real prototype for implementation of the used algorithm. Experimental results and practical setup are described and discussed for the PVG system with a SMC-MPPT.

This paper summarizes the main algorithms driving an entire PVG system obtained after long and extensive work, which dealt with theoretical and experimental efforts. Acquired results are very encouraging and suggest perspective experimental and theoretical studies for boosting PVG system performances. Moreover, this work can be extended to consider dynamic load types.

Conflicts of interest

The authors of this paper assure that they do not have any interest in DSPACE 1104 board and its software. They used DSPACE for research proposes only without any Relationship with the manufacturer or dealer.

Acknowledgments

The authors are very grateful to the Basque Government for their support of this work through the project S-PE13UN039 and to the University of the Basque Country (UPV/EHU) for its support through the projects GIU13/41 and UFI11/07. Also to the Tunisian Ministry of Higher Education and Scientific Research for their support of the research Unit, code UR11ES82.

References

[1] Farhat M, Flah A, Sbita L. Photovoltaic maximum power point tracking based on ANN control. Int Rev on Model Simul (IREMOS) 2014;7:474–80.
[2] Zakzouk NE, Abdelsalam AKA, Helal A, Williams BW. Modified variable-step incremental conductance maximum power point tracking technique for

photovoltaic systems. In: 39th Annual conference of the IEEE industrial electronics society. IECON; 2013. p. 1741–8.
[3] Hadji S, Gaubert J, Krim F. Maximum Power Point Tracking (MPPT) for photovoltaic systems using open circuit voltage and short circuit current. In: Int Conf Syst Control (ICSC). p. 87–92.
[4] El Khateb A, Rahim NA, Slvarj J, Uddin MN. Fuzzy logic controller based SEPIC converter for maximum power point tracking. IEEE Trans Ind Appl 2014;50:2349–58.
[5] Farhat M, Barambones O, Sbita L. Efficiency optimization of a DSP-based standalone PV system using a stable single input fuzzy logic controller. Renew Sustain Energy Rev 2015;49:907–20.
[6] Alqahtani A, Utkinin V. Self-optimization of photovoltaic system power generation based on sliding mode control. In: Proceedings of IECON'12. p. 3468–74.
[7] Levron Y, Shmilovitz D. Maximum power point tracking employing sliding mode control. IEEE Trans Circuits Syst 2013;60:724–31.
[8] Cid-Pastor A. Synthesis of loss-free resistors based on sliding-mode control and its applications in power processing. Control Eng Pract 2013;21:689–99.
[9] Oscar LL, Maria TP, Manel GA. New MPPT method for low-power solar energy harvesting. IEEE Trans Industr Electron 2010;57:3129–38.
[10] Elgendy M, Zahawi AB, Atkinson DJ. Comparison of directly connected and constant voltage controlled photovoltaic pumping systems. IEEE Trans Sustain Energy 2010;1:184–92.
[11] Xianwen G, Shaowu L, Rongfen G. Maximum power point tracking control strategies with variable weather parameters for photovoltaic generation systems. Sol Energy 2013;93:357–67.
[12] Jubaer A, Zainal S. An improved perturb and observe (P&O) maximum power point tracking (MPPT) algorithm for higher efficiency. Appl Energy 2015;150:97–108.
[13] Saravanan S, Ramesh Babu N. Maximum power point tracking algorithms for photovoltaic system – a review. Renew Sustain Energy Rev 2016;5:192–204.
[14] Mohammedi A, Mezzai N, Rekioua D, Rekioua T. Impact of shadow on the performances of a domestic photovoltaic pumping system incorporating an MPPT control: a case study in Bejaia, North Algeria. Energy Convers Manage 2014;84:20–9.
[15] Alsayid AB, Alsadi SY, Jallad JS, Dradi MH. Partial shading of PV system simulation with experimental results. Smart Grid Renewable Energy 2013;4:429–35.
[16] Sun Y, Chen S, Xie L, Hong R, Shen H. Investigating the impact of shading effect on the characteristics of a large-scale grid-connected PV power plant in Northwest China. Int J Photoenergy 2014. http://dx.doi.org/10.1155/2014/763106. 9 pages 763106.
[17] Gao L, Dougal RA, Liu S, Iotova AP. Parallel-connected solar PV system to address, partial and rapidly fluctuating shadow conditions. IEEE Trans Indust Electron 2009;56:1548–56.
[18] Anusuya C, Venkatasubramanian S. Design and implementation of solar power optimizer for DC distribution system using dual active bridge. Int J Adv Res Elect Electron Instrument Eng 2014;3:168–73.
[19] Muthuramalingam M, Manoharan PS. Comparative analysis of distributed MPPT controllers for partially shaded stand alone photovoltaic systems. Energy Convers Manage 2014;86:286–99.
[20] Rizzo S, Scelba G. ANN based MPPT method for rapidly variable shading conditions. Appl Energy 2015;145:124–32.
[21] Farhat M, Sbita L. Efficiency boosting for PV systems-MPPT intelligent control based. Energy Efficiency. Intech Publisher; 2015. http://dx.doi.org/10.5772/59399.
[22] Farhat M, Fleh A, Sbita L. Influence of photovoltaic DC bus voltage on the high speed PMSM drive. In: 38th Annual conference of the IEEE industrial electronics society 2012, 25–28 October, Montreal, Quebec, Canada.
[23] Muthuramalingam M, Manoharan PS. A photovoltaic power system using a high step-up converter for DC load applications. Energy Convers Manage 2014;86:286–99.
[24] Zhou Z, Holland PM, Igic P. MPPT algorithm test on a photovoltaic emulating system constructed by a DC power supply and an indoor solar panel. Energy Convers Manage 2014;85:460–9.
[25] Fernão PV, Romero-Cadaval E, Vinnikov D, Roasto I, Martins JF. Power converter interfaces for electrochemical energy storage systems – a review. Energy Convers Manage 2014;86:453–75.
[26] Shameem A, Fadi MAl, Saad M, Hazlie M. Fuzzy based controller for dynamic Unified Power Flow Controller to enhance power transfer capability. Energy Convers Manage 2014;79:652–65.
[27] Guerrero-Rodríguez NF, Alexis BB. Modelling, simulation and experimental verification for renewable agents connected to a distorted utility grid using a Real-Time Digital Simulation Platform. Energy Convers Manage 2014;84:108–21.
[28] Her TY, Chih JL, Qin CL. PSO based PI controller design for a solar charger system. Sci World J 2013:1–13.
[29] Farhat M, Barambones O, Sbita L, Fleh A. A robust MPP tracker based on sliding mode control for a photovoltaic pumping system. Int J Automat Comput, in press.
[30] Rújula AAB, Abián JAC. A novel MPPT method for PV systems with irradiance measurement. Sol Energy 2014;109:95–104.
[31] Liu C, Wu B, Cheung R. Advanced algorithm for MPPT control of photovoltaic system. In: Canadian Solar Buildings Conference Montreal, August 20–24, 2004.
[32] Abderrahim EF, Fouad G, Abdelmoinime M. Reference voltage optimizer for maximum power tracking in single-phase grid-connected photovoltaic systems. J Control Syst Eng 2013;12:57–66.
[33] Farhat M, Barambones O, Ramos JA, Durana JMG. Maximum power point tracking controller based on sliding mode approach. In: Actas de las XXXV Jornadas de Automática, Valencia, 3–5 de septiembre, 2014.
[34] Mathur Badrilal. Effect of shading on series and parallel connected solar PV modules. Modern Appl Sci 2009;3:32–41.
[35] Benyoucef As, Chouder A, Kara K, Silvestre S, Sahed OA. Artificial bee colony based algorithm for maximum power point tracking (MPPT) for PV systems operating under partial shaded conditions. Appl Soft Comput 2015;32:38–48.
[36] Farhat M, Sbita L. ANFIS controlled solar pumping system. i-Manager's J Electron Eng 2011;2:1–9.
[37] Farhat M, Barambones O, Fleh A, sbita L. Variable structure MPP controller for photovoltaic pumping system. Trans Inst Measure Control 2016:1–10.
[38] Rezk H, Eltamaly AM. A comprehensive comparison of different MPPT techniques for photovoltaic systems. Sol Energy 2015;112(February):1–11.
[39] Esram T, Chapman P. Comparison of photovoltaic maximum power point tracking techniques. IEEE Trans Energy Convers 2007;22:439–49.
[40] Fröhlich AA, Bezerra EA, Slongo LK. Experimental analysis of solar energy harvesting circuits efficiency for low power applications. Comput Electr Eng 2015;45:143–54.
[41] Valencia PAO, Paja CAR. Sliding-mode controller for maximum power point tracking in grid-connected photovoltaic systems. Energies 2015;8:12363–87. http://dx.doi.org/10.3390/en81112318.
[42] Herong G, Yajuan G, Huaibao W, Baoze W, Xiaoqiang G. Analysis and experimental verification of new power flow control for grid-connected inverter with LCL filter in microgrid. Sci World J 2014:1–8.

Please cite this article in press as: Farhat M et al. A new maximum power point method based on a sliding mode approach for solar energy harvesting. Appl Energy (2016), http://dx.doi.org/10.1016/j.apenergy.2016.03.055